

# Crossover in Electronic Specific Heat near Narrow-Sense Type-III Dirac Cones

Keita Kishigi

Faculty of Education, Kumamoto University, Kurokami 2-40-1, Kumamoto, 860-8555, Japan

Yasumasa Hasegawa

Department of Material Science, Graduate School of Material Science, University of Hyogo, Hyogo, 678-1297, Japan

(Dated: April 18, 2025)

Two-dimensional massless Dirac fermions exhibit Dirac cones, which are classified into three types: type-I, type-II, and type-III. In both type-I and type-II cones, the energy dispersion is linear in all momentum directions. Type-I cones are characterized by a non-overtilted structure, where the Dirac point serves as a local minimum (maximum) for the upper (lower) band. In contrast, type-II cones exhibit overtilted dispersions, leading to the coexistence of electron and hole pockets. At the critical tilt, the linear energy dispersion vanishes in one momentum direction, corresponding to a type-III Dirac cone. We further define a special case, termed the "narrow-sense" type-III cone, where not only the linear term but also quadratic and higher-order terms vanish, resulting in a completely flat dispersion along one direction. In this work, we numerically investigate the temperature ( $T$ )-dependence of the electronic specific heat ( $C$ ), as the Dirac cone is continuously tilted from type-I to narrow-sense type-III. A model with particle-hole symmetry is employed to ensure that the chemical potential ( $\mu$ ) remains temperature independent. Our results reveal a notable crossover in  $C$  near narrow-sense type-III, where  $C$  changes from  $C \propto T^2$  below the crossover temperature ( $T_{co}$ ) to  $C \propto T^{1/2}$  above  $T_{co}$ . This crossover is attributed to the energy-dependent structure of the density of states. The present findings suggest a feasible approach for experimentally probing the degree of Dirac cone tilting near the narrow-sense type-III limit.

## I. INTRODUCTION

Two-dimensional (2D) massless Dirac fermion systems are realized in materials such as graphene[1],  $\alpha$ -(BEDT-TTF) $_2$ I $_3$ [2–5], and  $\alpha$ -(BETS) $_2$ I $_3$ [6, 7], among others, where Dirac points and Dirac cones are present. These systems exhibit a variety of intriguing properties, particularly when two Dirac points merge[8–12].

One notable phenomenon is a topological phase transition to a normal insulating state that occurs upon the merging of two Dirac points. This has been theoretically predicted in systems such as honeycomb lattices[13, 14], VO $_2$ /TiO $_2$  nanostructures[15], and  $\alpha$ -(BEDT-TTF) $_2$ I $_3$ [16]. This merging point is termed the semi-Dirac point[15]. Experimental realizations of this transition and a semi-Dirac point have been reported in artificial systems including ultracold atoms in optical lattices [8], photonic resonator lattices [9], and polariton systems in semiconductor micropillar lattices [10, 11]. More recently, evidence of a semi-Dirac point has been reported in real materials such as ZrSiS [12].

Near the merging of two Dirac points, a crossover behavior in the temperature ( $T$ )-dependence of the electronic specific heat ( $C$ ) has been identified through numerical calculations [17]. Specifically,  $C \propto T^2$  at low temperatures and  $C \propto T^{3/2}$  at higher temperatures, separated by a crossover temperature ( $T_{co}$ ). This crossover is caused by the energy ( $\varepsilon$ )-dependence of the density of states (DOS) [ $D(\varepsilon)$ ], where  $D(\varepsilon) \propto |\varepsilon - \varepsilon_F|$  near the Fermi energy ( $\varepsilon_F$ ) (as expected for 2D Dirac systems) and  $D(\varepsilon) \propto |\varepsilon - \varepsilon_F|^{1/2}$  far from  $\varepsilon_F$  (as expected for 2D semi-Dirac systems). As two Dirac points approach each other,  $T_{co}$  shifts to lower values and eventually vanishes upon merging. This crossover thus serves as an important indicator of a topological phase transition in 2D Dirac systems[17].

The experimental observation of the electronic specific

heat,  $C$ , has been achieved[5] only in bulk materials such as  $\alpha$ -(BEDT-TTF) $_2$ I $_3$ , where  $C \propto T^{1.8}$  has been measured and is close to expected  $C \propto T^2$ . However, the crossover in  $C$  associated with the topological phase transition has not yet been observed. It may be detectable under uniaxial strain.

The concept of a tilted Dirac cone has been extensively studied in 2D massless Dirac systems, particularly in  $\alpha$ -(BEDT-TTF) $_2$ I $_3$ , both theoretically [18, 19] and experimentally [20]. Tilted cones are typically classified into type-I, -II, and -III. Type-I cones are tilted but not overtilted, type-II are overtilted, and type-III are critically tilted where the linear dispersion vanishes along one-direction. Type-III Dirac cones have been proposed in systems including Zn $_2$ In $_2$ [21], laser-irradiated black phosphorus[22], and Ni $_3$ In $_2$ X $_2$  ( $X = S, Se$ )[23], based on first-principles calculations.

Recently, type-III has drawn attention due to their analogy to black holes in condensed matter systems[24–26]. Theoretical studies have revealed that type-III systems exhibit unique transport properties distinct from those of types-I and -II [27].

In this study, we focus on the electronic specific heat in the vicinity of "narrow-sense type-III" Dirac cones, where the linear and higher-order terms vanishes. We adopt a minimal model given by

$$\varepsilon = \varepsilon_F + \alpha k_y \pm \hbar v_F \sqrt{k_x^2 + k_y^2}, \quad (1)$$

where  $h$  is Planck's constant,  $\hbar = h/(2\pi)$ ,  $v_F$  is the Fermi velocity, and the parameter,  $\alpha$ , characterizes the tilting of the Dirac cone along the  $k_y$  direction. We define a dimensionless tilting parameter as  $\tilde{\alpha} = \alpha/(\hbar v_F)$ , and the system is classified as type-I for  $|\tilde{\alpha}| < 1$ , narrow-sense type-III for  $|\tilde{\alpha}| = 1$ , and type-II for  $|\tilde{\alpha}| > 1$ . Figures 1 and 2 show the energy dispersion for representative values of  $\tilde{\alpha}$  in each regime.

In the narrow-sense type-III case, the dispersion becomes flat along the  $k_y$  direction at  $k_x = 0$ . In this work, the Fermi

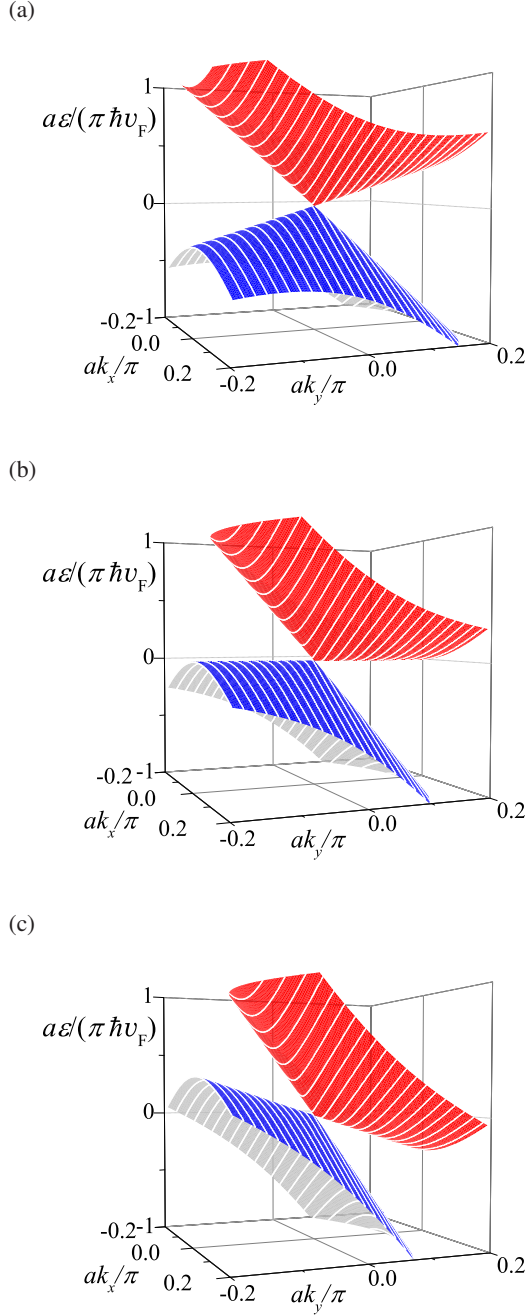


FIG. 1. (Color online) The energy bands of 2D type-I (a), narrow-sense type-III (b), and type-II (c) Dirac described by Eq. (1), where we take  $\varepsilon_F = 0$  and  $\tilde{\alpha} = -0.5$  for (a),  $\tilde{\alpha} = -1$  for (b), and  $\tilde{\alpha} = -1.5$  for (c). The Dirac point ( $\mathbf{k}_D$ ) is  $\mathbf{k}_D = (0, 0)$  and the Dirac cone is tilted to the  $k_y$ -axis.

energy  $\varepsilon_F$  is set to the Dirac point in the type-I case and to the flat band segment in the narrow-sense type-III case. Accordingly, the electron filling is fixed at half-filling,  $\nu = 1/2$ .

To incorporate higher-order effects near the critical tilting, we also consider a modified model:

$$\varepsilon = \varepsilon_F + \alpha k_y + \alpha'_2 k_y^2 \pm \hbar v_F \sqrt{k_x^2 + (\alpha k_y - \alpha''_2 k_y^2)^2}, \quad (2)$$

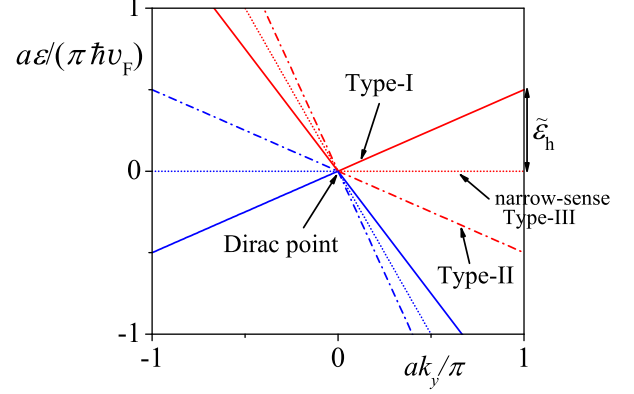


FIG. 2. (Color online) The energy dispersions of type-I (solid lines), narrow-sense type-III (dotted lines), and type-II (dash-dot lines) shown in Figs. 1(a), (b) and (c) are viewed along the  $k_x$ -axis, respectively. The height of the Dirac cone ( $\tilde{\varepsilon}_h$ ) from  $k_x = 0$  to  $\pi/a$  (or  $-\pi/a$ ) is given by  $\tilde{\varepsilon}_h = \tilde{\alpha} \pm 1$ , where + and - signs correspond to  $\tilde{\alpha} < 0$  and  $\tilde{\alpha} > 0$ , respectively. For type-I with  $\tilde{\alpha} = -0.5$ ,  $\tilde{\varepsilon}_h = 0.5$ . For  $\tilde{\alpha} = 1$  or  $-1$ , the Dirac cone becomes narrow-sense type-III.

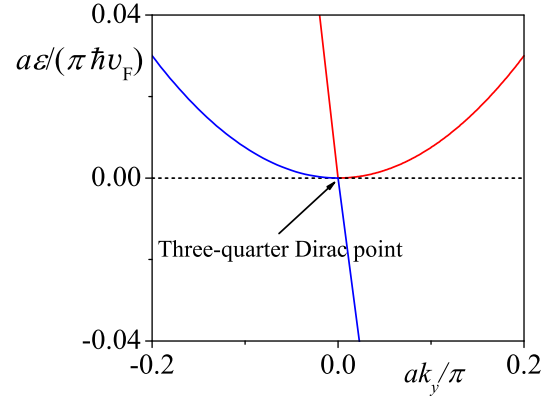


FIG. 3. (Color online) The energy dispersion of three-quarter Dirac described by Eq. (2) with  $\tilde{\alpha} = -1$ ,  $\varepsilon_F = 0$ ,  $\alpha'_2 = \hbar v_F/2$ , and  $\alpha''_2 = \hbar v_F/4$  is viewed along the  $k_x$ -axis.

where  $\alpha'_2$  and/or  $\alpha''_2$  are nonzero for  $|\tilde{\alpha}| = 1$ . This model exhibits three-quarter-Dirac cone[28], characterized by quadratic dispersion in one direction and linear dispersion in the other three directions. Such a feature appears in the tight-binding model for  $\alpha$ -(BEDT-TTF) $_2$ I $_3$  under the uniaxial pressure of 2.3 kbar[28]. Three-quarter-Dirac cone can be regarded as a more general form of the type-III Dirac cone, because the energy dispersion exhibits locally flat behavior at three-quarter-Dirac point along the  $k_y$ -axis, as shown in Fig. 3.

The electronic structures of narrow-sense type-III and three-quarter Dirac cones exhibit fundamentally different magnetic and thermodynamic properties. For instance, the Landau quantization of the upper band in the three-quarter

Dirac system follows  $E_n \propto B^{4/5}$ [28], whereas in narrow-sense type-III it scales as  $B^2$ . In this work, we restrict our analysis to the narrow-sense type-III case based on Eq. (1), to clarify the specific heat behavior near the critical tilting.

Importantly, while Eq. (1) applies for type-II ( $|\tilde{\alpha}| > 1$ ), in that regime electron and hole pockets typically emerge, making the linear approximation invalid. We therefore limit our analysis of  $C$  to the vicinity of the type-I/type-III boundary.

In 2D systems for type-I and narrow-sense type-III, the DOS is given by (see Appendix A)

$$D(\varepsilon) \propto \begin{cases} |\varepsilon - \varepsilon_F| & \text{for type-I Dirac,} \\ |\varepsilon - \varepsilon_F|^{-1/2} & \text{for narrow-sense type-III Dirac.} \end{cases} \quad (3)$$

The DOS diverges at  $\varepsilon = \varepsilon_F$  in narrow-sense type-III, because the electronic states are concentrated in the flat dispersion at  $k_x = 0$ .

When the Dirac cone is tilted from type-I to narrow-sense type-III, the DOS,  $D(\varepsilon)$ , is shown in Fig. 4 (a). For  $-1 < \tilde{\alpha} \leq -0.999$ ,  $D(\varepsilon)$  follows  $D(\varepsilon) \propto |\varepsilon - \varepsilon_F|$  near  $\varepsilon_F$  and  $D(\varepsilon) \propto |\varepsilon - \varepsilon_F|^{-1/2}$  far from  $\varepsilon_F$ . In this situation, the crossover, where  $C$  transitions from  $C \propto T^2$  below  $T_{co}$  to  $C \propto T^{1/2}$  above  $T_{co}$ , is expected near narrow-sense type-III.

## II. CALCULATION OF ELECTRONIC SPECIFIC HEAT

While Coulomb interactions[29–31] have been theoretically accounted for in graphene, such as demonstrating logarithmic corrections to thermodynamic properties[30], we assume that the influence of Coulomb interactions is negligible compared to that of the tilting of Dirac cones.

The internal energy per site,  $U$ , at temperature,  $T$ , is given by

$$U = \frac{1}{N} \sum_{i=\pm} \sum_{\mathbf{k}} \varepsilon_i(\mathbf{k}) f[\varepsilon_i(\mathbf{k})], \quad (4)$$

where  $\varepsilon_i(\mathbf{k})$  denotes the energy eigenvalue of band  $i$ , and  $f[\varepsilon_i(\mathbf{k})]$  is the Fermi-Dirac distribution function. Here,  $N = 2N_k$  with  $N_k$  representing the number of  $\mathbf{k}$  points sampled within the first Brillouin zone.

The electronic specific heat at constant volume,  $C$ , is obtained by taking the temperature derivative of the internal energy:

$$C = \frac{dU}{dT}. \quad (5)$$

In this study, we ignore the spin degree of freedom, which does not affect the power-law behavior of  $C$  with respect to  $T$ . Including spin would simply introduce a factor of two on the right-hand side of Eq. (5).

## III. ANALYTIC CALCULATIONS IN SPECIAL CASES WITH PARTICLE-HOLE SYMMETRY

We consider the following generalized DOS with particle-hole symmetry:

$$D(\varepsilon) = ND_0 |\varepsilon - \varepsilon_F|^\beta, \quad (6)$$

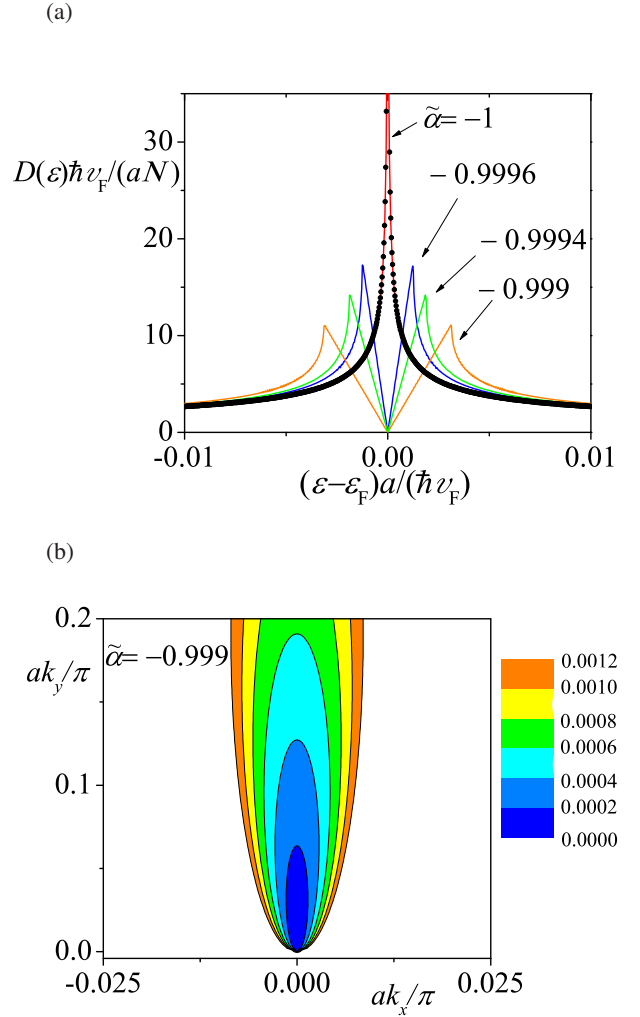


FIG. 4. (Color online) (a) The DOS for Dirac systems evolving from type-I to narrow-sense type-III regimes. The blue, green, and orange curves correspond to numerical calculations using Eq. (1) with  $\tilde{\alpha} = -0.9996, -0.9994$ , and  $-0.999$ , respectively. Black circles represent the numerical result for  $\tilde{\alpha} = -1$ , obtained within the first Brillouin zone defined by  $-\pi/a \leq k_x < \pi/a$  and  $-\pi/a \leq k_y < \pi/a$ . The red solid line denotes the analytical expression given by Eq. (A5), which is in excellent agreement with the numerical data for  $\tilde{\alpha} = -1$ . (b) Contour plot of the upper energy band described by Eq. (1) for  $\tilde{\alpha} = -0.999$  at  $\varepsilon_F = 0$ . Near  $\varepsilon \approx \varepsilon_F$ , the electronic states are localized around two Dirac points. For higher energies (e.g.,  $\varepsilon \gtrsim 0.0008$ ), the states extend along a line-shaped region centered around  $k_x \approx 0$  and  $0 < k_y \leq \pi/a$ . A similar behavior is observed in the lower band for  $\varepsilon \ll \varepsilon_F$ , where states are distributed along a line near  $k_x \approx 0$  and  $-\pi/a \leq k_y < 0$ . These features underlie the characteristic energy dependence of the DOS for  $\tilde{\alpha} = -0.999$  shown in panel (a).

where  $D_0$  and  $\beta$  are constant. For Eq. (6), we derive an analytical expression for  $C$  in Appendix B, which is presented in Eq. (B4). This leads to characteristic power-law  $T$ -dependences of  $C$  as follows:

$$C \propto \begin{cases} T^2 & \text{for type-I Dirac,} \\ T^{1/2} & \text{for narrow-sense type-III Dirac.} \end{cases} \quad (7)$$

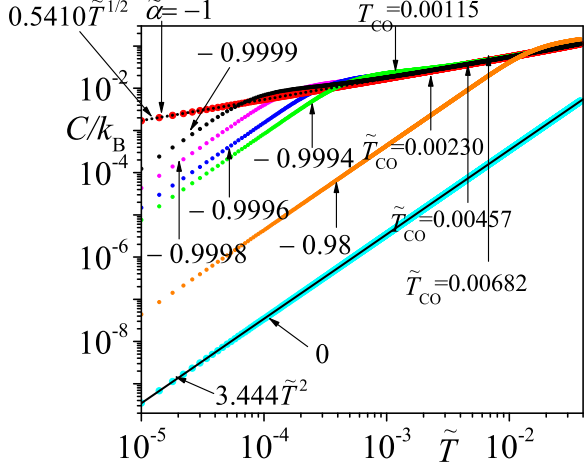


FIG. 5. (Color online) Electronic specific heats, calculated numerically from Eq. (1), are shown as red circles and other colored circles (black, pink, blue, green, orange, sky blue) corresponding to values of  $\tilde{\alpha} = -1, -0.9999, -0.9998, -0.9996, -0.9994, -0.98,$  and  $0$ . A dotted black line and a black solid line represent  $0.5410\tilde{T}^{1/2}$  from Eq. (B6) and  $3.444\tilde{T}^2$  from Eq. (B5), respectively. The estimated crossover temperatures,  $\tilde{T}_{co}$ , are  $0.00115, 0.00230, 0.0457,$  and  $0.00682$  for  $\tilde{\alpha} = -0.9999, -0.9998, -0.9996,$  and  $-0.9994$ .

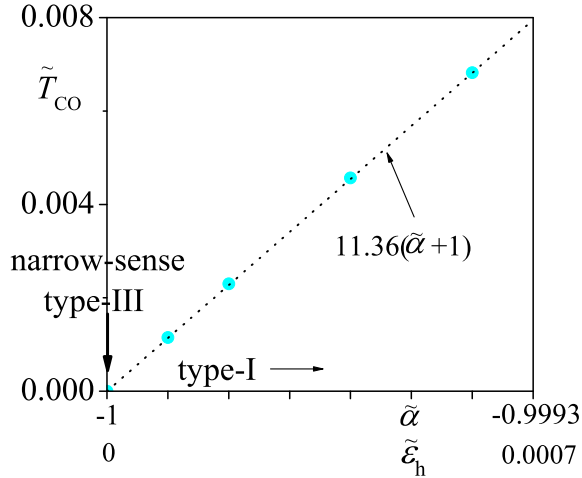


FIG. 6. (Color online) Crossover temperatures as a function of  $\tilde{\alpha}$  (or  $\theta$ ) from type-I to narrow-sense type-III (sky blue circles). The sky blue circles are fitted well as  $\tilde{T}_{co} = 11.36(\tilde{\alpha} + 1)$  or  $\tilde{T}_{co} = 11.36\tilde{\epsilon}_h$ .

#### IV. NUMERICAL CALCULATIONS FOR DIRAC CONE TILTING FROM TYPE I TO TYPE III

Since the Dirac points appear as a pair at the time-reversal-invariant-momenta in general, we multiply the numerically obtained  $C$  by a factor of two. The momentum summation is

performed over the first Brillouin zone of a square lattice, defined by  $-\pi/a \leq k_x < \pi/a$  and  $-\pi/a \leq k_y < \pi/a$ . The power-law behavior of  $C$  as a function of  $T$  remains unchanged even if any Brillouin zone is chosen.

Throughout this work, we employ a dimensionless temperature defined as

$$\tilde{T} = \frac{ak_B T}{\hbar v_F}, \quad (8)$$

where  $k_B$  is the Boltzmann constant. For graphene, it has been known[32] that  $\hbar v_F = \sqrt{3}at/2$ , where  $t$  is nearest transfer integrals. Based on first-principles calculations[33],  $t$  is estimated to be approximately 2.97 eV, implying that  $\tilde{T} = 0.0001$  corresponds to approximately 2.98 K.

Figures 5 displays the numerically calculated  $C$ . For type-I ( $\tilde{\alpha} = 0$ ),  $C$  (sky blue circles) is well fitted by the analytical expression in Eq. (B5) (black solid line). Similarly, for narrow-sense type-III ( $\tilde{\alpha} = -1$ ),  $C$  (red circles) is accurately fitted by Eq. (B6) (dotted black line).

Near narrow-sense type-III regime ( $-0.9999 \leq \tilde{\alpha} \leq -0.98$ ), a crossover behavior is observed in the  $T$ -dependence of  $C$ . At low temperatures,  $C \propto \tilde{T}^2$ , as expected for type-I, while at higher temperatures, it transitions to  $C \propto \tilde{T}^{1/2}$ , characteristic of the narrow-sense type-III. This crossover arises from the change in  $\epsilon$ -dependence of  $D(\epsilon)$  (see Fig. 4). The low temperature behavior of  $C$  is primarily governed by  $D(\epsilon)$  near  $\epsilon_F$ , while the high temperature behavior of  $C$  reflects contributions from states farther away from  $\epsilon_F$ .

The crossover temperature,  $\tilde{T}_{co}$ , is defined as the temperature at which the specific heat for  $\tilde{\alpha} = -0.9999, -0.9998, -0.9996,$  and  $-0.9994$  (black, pink, blue, and green circles in Fig. 5) deviate by less than 5.0% from the result for  $\tilde{\alpha} = -1$  (red circles in Fig. 5). At  $\tilde{T}_{co}$ , the power-law exponent governing the temperature dependence of  $C$  changes. As shown in Fig. 6,  $\tilde{T}_{co}$  increases linearly with  $\tilde{\alpha}$ , or equivalently with the dimensionless height of the Dirac cone  $\tilde{\epsilon}_h$ , indicating that  $\tilde{T}_{co} \propto \tilde{\epsilon}_h$ .

#### V. CONCLUSIONS

When the Dirac cone is tilted from type-I to narrow-sense type-III in 2D Dirac fermions, a notable crossover appears in the  $T$ -dependence of the electronic specific heat,  $C$ . Assuming particle-hole symmetry is preserved (or its breaking does not significantly influence the  $T$ -dependence of the chemical potential  $\mu$ ), the specific heat exhibits a transition from  $C \propto T^2$  at low temperatures ( $T < T_{co}$ ) to  $C \propto T^{1/2}$  at higher temperatures ( $T > T_{co}$ ). The crossover temperatures,  $T_{co}$ , is proportional to the height of the Dirac cone and approaches zero in the narrow-sense type-III limit. This behavior offers a practical means to experimentally probe Dirac cone tilting near narrow-sense type-III systems when the Fermi energy lies at the Dirac point and the  $T$ -dependence of  $\mu$  is negligibly small.

A nearly flat Dirac cone with the Fermi energy positioned close to the Dirac point in  $\alpha$ -(BETS)<sub>2</sub>I<sub>3</sub> has recently been identified through first-principles density functional theory[7]. If the observed tilting corresponds to narrow-sense type-III



and the  $T$ -dependence of  $\mu$  is negligibly small, the predicted crossover and the associated  $T_{co}$  should be experimentally observable.

In the present analysis, the  $T$ -dependence of  $\mu$  is ignored owing to particle-hole symmetry. However, in certain Dirac fermions where particle-hole symmetry is substantially broken [e.g., the tight-binding model with the honeycomb lattice including next-nearest neighbor hoppings[34], three-quarter-Dirac, and  $\alpha$ -(BEDT-TTF)<sub>2</sub>I<sub>3</sub>[17]], the  $T$ -dependence of  $\mu$  must be taken into account when evaluating  $C$ .

To fully understand the thermal and magnetic properties of type-III Dirac systems, a clear distinction between narrow-sense type-III and three-quarter-Dirac dispersions is essential. In particular, the differences in the DOS and Landau level structures may lead to distinct experimental signatures. Further theoretical investigations based on realistic models and first-principles calculations will be valuable for developing a more comprehensive understanding of these systems.

## Appendix A: Density of states for characteristic Dirac systems

In this Appendix, we present expressions for the DOS for two Dirac-type systems that exhibit particle-hole symmetry.

### 1. 2D type-I Dirac fermions

For 2D type-I Dirac fermions on a square lattice, where the first Brillouin zone is defined by  $-\pi/a \leq k_x < \pi/a$  and  $-\pi/a \leq k_y < \pi/a$ , the DOS can be evaluated analytically for the case  $\alpha = 0$  in Eq. (1). In this limit, the low-energy dispersion around each Dirac point is isotropic and linear, characterized by the Fermi velocity,  $v_F$ . The resulting DOS reads

$$D(\varepsilon) = \frac{N}{\pi} \left( \frac{a}{\hbar v_F} \right)^2 |\varepsilon - \varepsilon_F|. \quad (\text{A1})$$

The overall factor is doubled due to the presence of two inequivalent Dirac points.

### 2. 2D narrow-sense type-III Dirac fermions

In the case of 2D narrow-sense type-III Dirac fermions, the dispersion is obtained by setting  $\alpha = -\hbar v_F$  in Eq. (1). Expanding around the Dirac point  $(k_x, k_y) = (0, 0)$  yields

$$\varepsilon \simeq \varepsilon_F \pm \frac{\hbar v_F}{2k_y^0} k_x^2, \quad (\text{A2})$$

at fixed  $k_y = k_y^0$ . This expansion is valid in the region  $|k_x| \ll |k_y^0|$ . When  $k_y^0 = 0$ , the dispersion becomes linear in  $k_x$ , i.e.,  $\varepsilon = \varepsilon_F \pm \hbar v_F |k_x|$ . For  $k_y^0 \neq 0$ , the  $k_x$ -dependence resembles that of one-dimensional free electrons, with an effective mass controlled by  $k_y^0$  [see Fig. 7].

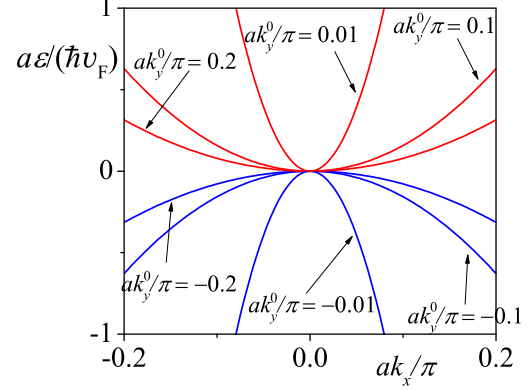


FIG. 7. (Color online) Energy dispersion along the  $k_x$ -axis for several values of  $k_y^0$ , based on Eq. (A2), with  $\varepsilon_F = 0$ . The red and blue curves correspond to the upper and lower bands, respectively.

By using Eq. (1), the constant-energy contour for the upper band is given by

$$k_y = \frac{1}{2} \left( \frac{\hbar v_F}{\varepsilon - \varepsilon_F} k_x^2 - \frac{\varepsilon - \varepsilon_F}{\hbar v_F} \right). \quad (\text{A3})$$

The number of states  $[\Omega]$  between  $\varepsilon_F$  and  $\varepsilon$  is obtained by integrating over the area enclosed by Eq. (A3) and the Brillouin zone boundary  $k_y = \pi/a$ . For  $\varepsilon \simeq \varepsilon_F$ , this gives

$$\Omega \simeq \frac{N}{3} \sqrt{\frac{2a}{\pi \hbar v_F}} \sqrt{|\varepsilon - \varepsilon_F|}. \quad (\text{A4})$$

Considering the existence of two Dirac points, the DOS in the narrow-sense type-III is

$$\begin{aligned} D(\varepsilon) &= 2 \frac{d\Omega}{d\varepsilon} \\ &= \frac{N}{3} \sqrt{\frac{2a}{\pi \hbar v_F}} |\varepsilon - \varepsilon_F|^{-1/2}, \end{aligned} \quad (\text{A5})$$

which diverges at  $\varepsilon = \varepsilon_F$ .

## Appendix B: Analytical expression of electronic specific heat for generalized density of states

We derive an analytical expression for the electronic specific heat,  $C$ , corresponding to Eq. (6) under the condition of half filling,  $\nu = 1/2$ . Starting from Eq. (4), the internal energy per site,  $U$ , can be rewritten in terms of  $D(\varepsilon)$  as

$$U = \frac{1}{N} \int_{-\infty}^{\infty} (\varepsilon - \mu) D(\varepsilon) f(\varepsilon) d\varepsilon + \mu \nu, \quad (\text{B1})$$

where  $\mu$  is the chemical potential. Owing to the particle-hole symmetry of systems described by Eq. (6), the chemical potential remains temperature-independent, i.e.,  $\mu = \varepsilon_F$  for all  $T$ . The second term in Eq. (B1) does not contribute to the

specific heat. Consequently, it can be omitted in the following analysis.

Substituting Eq. (6) into Eq. (B1) and changing variables to  $x = (\varepsilon - \mu)/(k_B T)$ , we obtain

$$C = k_B D_0 \tilde{T}^{\beta+1} \int_{-\infty}^{\infty} \frac{|x|^{\beta+2} e^x}{(e^x + 1)^2} dx. \quad (\text{B2})$$

The integral in Eq. (B2) can be evaluated analytically as

$$\begin{aligned} \int_{-\infty}^{\infty} \frac{|x|^{\beta+2} e^x}{(e^x + 1)^2} dx &= 2(\beta + 2) \sum_{k=0}^{\infty} \frac{(-1)^k}{(1+k)^{\beta+2}} \int_0^{\infty} y^{\beta+1} e^{-y} dy \\ &= 2(\beta + 2) \left(1 - 2^{-(\beta+1)}\right) \zeta(\beta + 2) \Gamma(\beta + 2), \end{aligned} \quad (\text{B3})$$

where  $\zeta(x)$  and  $\Gamma(x)$  are the Riemann zeta and gamma functions, respectively.

Substituting Eq. (B3) into Eq. (B2), we obtain the final expression for the electronic specific heat:

$$C = 2k_B D_0 (\beta + 2) \left(1 - 2^{-(\beta+1)}\right) \zeta(\beta + 2) \Gamma(\beta + 2) \left(\frac{\hbar v_F}{a}\right)^{\beta+1} \tilde{T}^{\beta+1}. \quad (\text{B4})$$

This result confirms that the specific heat scales as  $\tilde{T}^{\beta+1}$  for a DOS of the form  $D(\varepsilon) \propto |\varepsilon - \varepsilon_F|^\beta$ .

### 1. Electronic Specific heat for characteristic Dirac systems

Using Eqs. (A1) and (A5), we summarize the low temperature behavior of the electronic specific heat,  $C$ , for two Dirac-type systems:

#### • 2D type-I Dirac fermions:

$$\begin{aligned} C &= \frac{9}{2\pi} \zeta(3) \Gamma(3) k_B \tilde{T}^2 \\ &\simeq 3.444 k_B \tilde{T}^2, \end{aligned} \quad (\text{B5})$$

#### • 2D narrow-sense type-III Dirac fermions:

$$\begin{aligned} C &= \sqrt{\frac{2}{\pi}} \left(1 - 2^{-1/2}\right) \zeta(3/2) \Gamma(3/2) k_B \tilde{T}^{1/2} \\ &\simeq 0.5410 k_B \tilde{T}^{1/2}. \end{aligned} \quad (\text{B6})$$

- 
- [1] K. S. Novoselov, A. K. Geim, S. V. Morozov, D. Jiang, M. I. Katsnelson, I. V. Grigorieva, S. V. Dubonos, and A. A. Firsov, Two-dimensional gas of massless Dirac fermions in graphene, *Nature* **438**, 197 (2005).
- [2] K. Kajita, Y. Nishio, N. Tajima, Y. Suzumura and A. Kobayashi, Molecular Dirac fermion systems -Theoretical and experimental approaches-, *J. Phys. Soc. Jpn.* **83**, 072002 (2014).
- [3] T. Osada, Negative interlayer magnetoresistance and zero-mode Landau level in multilayer Dirac electron system, *J. Phys. Soc. Jpn.* **77**, 084711 (2008).
- [4] M. Hirata, K. Ishikawa, K. Miyagawa, K. Kanoda and M. Tamura,  $^{13}\text{C}$  NMR study on the charge-disproportionated conducting state in the quasi-two-dimensional organic conductor  $\alpha$ -(BEDT-TTF) $_2\text{I}_3$ , *Phys. Rev. B* **84**, 125133 (2011).
- [5] T. Konoike, K. Uchida and T. Osada, Specific heat of the multilayered massless Dirac fermion system, *J. Phys. Soc. Jpn.* **81**, 043601 (2012).
- [6] Y. Kawasaki, H. Masuda, M. Uebe, H. M. Yamamoto, R. Kato, Y. Nishio, and N. Tajima, Pressure-induced phase switching of Shubnikov-de Haas oscillations in the molecular Dirac fermion system  $\alpha$ -(BETS) $_2\text{I}_3$ , *Phys. Rev. B* **103**, 205140 (2021).
- [7] S. Kitou, T. Tsumuraya, H. Sawahata, F. Ishii, K. I. Hiraki, T. Nakamura, N. Katayama, and H. Sawa, Ambient-pressure Dirac electron system in the quasi-two-dimensional molecular conductor  $\alpha$ -(BETS) $_2\text{I}_3$ , *Phys. Rev. B* **103**, 035135 (2021).
- [8] L. Tarruell, D. Greif, T. Uehlinger, G. Jotzu, and T. Esslinger, Creating, moving and merging Dirac points with a Fermi gas in a tunable honeycomb lattice, *Nature* **483**, 302 (2012).
- [9] M. Bellec, U. Kuhl, G. Montambaux, and F. Mortessagne, Topological transition of Dirac points in a microwave experiment, *Phys. Rev. Lett.* **110**, 033902 (2013).
- [10] M. Milićević, G. Montambaux, T. Ozawa, O. Jamadi, B. Real, I. Sagnes, A. Lemaître, L. Le Gratiet, A. Harouri, J. Bloch, and A. Amo, Type-III and tilted Dirac cones emerging from flat bands in photonic orbital graphene, *Phys. Rev. X* **9**, 031010 (2019).
- [11] B. Real, O. Jamadi, M. Milićević, N. Pernet, P. St-Jean, T. Ozawa, G. Montambaux, I. Sagnes, A. Lemaître, L. Le Gratiet, A. Harouri, S. Ravets, J. Bloch, and A. Amo, Semi-Dirac transport and anisotropic localization in polariton honeycomb lattices, *Phys. Rev. Lett.* **125**, 186601 (2020).
- [12] Yinming Shao, Seongphill Moon, A. N. Rudenko, Jie Wang, Jonah Herzog-Arbeitman, Mykhaylo Ozerov, David Graf, Zhiyuan Sun, Raquel Queiroz, Seng Huat Lee, Yanglin Zhu, Zhiqiang Mao, M. I. Katsnelson, B. Andrei Bernevig, Dmitry Smirnov, Andrew J. Millis, and D. N. Basov, Semi-Dirac Fermions in a Topological Metal, *Phys. Rev. X* **14**, 041057 (2024).
- [13] Y. Hasegawa, R. Konno, H. Nakano, and M. Kohmoto, Zero modes of tight-binding electrons on the honeycomb lattice, *Phys. Rev. B* **74**, 033413 (2006).
- [14] P. Dietl, F. Piéchon, and G. Montambaux, New magnetic field dependence of Landau levels in a graphenelike structure, *Phys. Rev. Lett.* **100**, 236405 (2008).
- [15] S. Banerjee, R. R. P. Singh, V. Pardo, and W. E. Pickett, Tight-binding modeling and low-energy behavior of the semi-Dirac point, *Phys. Rev. Lett.* **103**, 016402 (2009).
- [16] Y. Suzumura, T. Morinari and F. Piechon, Mechanism of Dirac point in  $\alpha$  type organic conductor under pressure, *J. Phys. Soc. Jpn.* **82**, 023708 (2013).
- [17] K. Kishigi, K. Tsukidashi, and Y. Hasegawa, Observable Precursor of Topological Phase Transition: Temperature-dependent Electronic Specific Heat in Two-dimensional Dirac Fermions, *J. Phys. Soc. Jpn.* **92**, 104601 (2023).
- [18] S. Katayama, A. Kobayashi and Y. Suzumura, Pressure-induced zero-gap semiconducting state in organic conductor  $\alpha$ -(BEDT-TTF) $_2\text{I}_3$  salt, *J. Phys. Soc. Jpn.* **75**, 054705 (2006).

- [19] H. Kino and T. Miyazaki, First-principles study of electronic structure in  $\alpha$ -(BEDT-TTF)<sub>2</sub>I<sub>3</sub> at ambient pressure and with uniaxial strain, *J. Phys. Soc. Jpn.* **75**, 034704 (2006).
- [20] M. Hirata, K. Ishikawa, K. Miyagawa, M. Tamura, C. Berthier, D. Basko, A. Kobayashi, G. Matsuno, and K. Kanoda., Observation of an anisotropic Dirac cone reshaping and ferrimagnetic spin polarization in an organic conductor, *Nature Communications* **7**, 12666 (2016).
- [21] H. Huang, K.-H. Jin, and F. Liu, Black-Hole Horizon in the Dirac Semimetal Zn<sub>2</sub>In<sub>2</sub>S<sub>5</sub>, *Phys. Rev. B* **98**, 121110(R) (2018).
- [22] H. Liu, J.-T. Sun, C. Cheng, F. Liu, and S. Meng, Photoinduced Nonequilibrium Topological States in Strained Black Phosphorus, *Phys. Rev. Lett.* **120**, 237403 (2018).
- [23] C. Sims, Analogous Black Holes in Type-III Dirac Semimetal Ni<sub>3</sub>In<sub>2</sub>X<sub>2</sub> ( $X = S, Se$ ), *Crystals*, **13**, 847 (2023).
- [24] G. E. Volovik, Black hole and hawking radiation by type-II Weyl fermions, *JETP Lett.* **104**, 645 (2016).
- [25] G. E. Volovik and K. Zhang, Lifshitz Transitions, Type-II Dirac and Weyl Fermions, Event Horizon and All That, *J. Low Temp. Phys.* **189**, 276 (2017).
- [26] G. E. Volovik, Exotic Lifshitz transitions in topological materials, *Phys. Usp.* **61**, 89 (2018).
- [27] T. Mizoguchi, H. Matsuura, and M. Ogata, Thermoelectric transport of type-I, II, and III massless Dirac fermions in a two-dimensional lattice model, *Phys. Rev. B* **105**, 205203 (2022).
- [28] K. Kishigi, and Y. Hasegawa, Three-quarter Dirac points, Landau levels, and magnetization in  $\alpha$ -(BEDT-TTF)<sub>2</sub>I<sub>3</sub>, *Phys. Rev. B* **96**, 085430 (2017).
- [29] O. Vafek, Anomalous Thermodynamics of Coulomb-Interacting massless Dirac fermions in Two Spatial Dimensions, *Phys. Rev. Lett.* **98**, 216401 (2007).
- [30] D. E. Sheehy and J. Schmalian, Quantum critical scaling in graphene, *Phys. Rev. Lett.* **99**, 226803 (2007).
- [31] V. N. Kotov, B. Uchoa, V. M. Pereira, F. Guinea, and A. H. Castro Neto, Electron-electron interactions in graphene: current status and perspectives, *Rev. Mod. Phys.* **84**, 1067 (2012).
- [32] P. R. Wallace, The Band theory of graphite, *Phys. Rev.* **71**, 622 (1947).
- [33] S. Reich, J. Maultzsch, C. Thomsen, and P. Ordejon, Tight-binding description of graphene, *Phys. Rev. B* **66**, 035412 (2002).
- [34] K. Kishigi, K. Ueno, E. Miyamoto, and Y. Hasegawa, Dirac cones on the generalized honeycomb lattice, *J. Phys.: Conference Series* **334**, 012047 (2011).